Synthesis, characterization and properties of sulfate-modified silver carbonate with enhanced visible light photocatalytic performance†

Sara Ghazi,[ab] Benaissa Rhouta, [ID] *[a] Claire Tendero [ID] [b] and Francis Maury[b]

Sulfate-modified Ag_2CO_3 was successfully synthesized *via* a simple precipitation method. Its visible light photocatalytic performance against the removal of Orange G was found to be significantly enhanced in comparison with the one of pure Ag_2CO_3. While SO_4^{2-}-Ag_2CO_3 ensured a removal efficiency of 100% of OG within 30 min, the unmodified Ag_2CO_3 exhibited a degradation threshold at hardly 60%. Likewise, the degradation rate constant in the presence of SO_4^{2-}-Ag_2CO_3 photocatalyst was assessed to be twice that determined upon the involvement of pristine Ag_2CO_3. Furthermore, Total Organic Carbon (TOC) measurements evidenced the occurrence of a quasi-total mineralization of the dye pollutant upon the use of SO_4^{2-}-Ag_2CO_3 photocatalyst. Scavenger experiments highlighted the dominant role of photo-induced h^+ along with $^\bullet O_3^-$ ozonide radicals in the OG photocatalytic oxidation mechanism. Reuse cycles revealed that the modification by SO_4^{2-} is a promising route to improve the stability of silver carbonate against photocorrosion. All these improvements could be ascribed to electronic transfer from the upper SO_4^{2-} HOMO to the lower Ag_2CO_3 conduction band.

1 Introduction

Great attention was recently paid to silver based photocatalysts such as Ag_2O,[1] AgX (X = Cl, I and Br),[2] Ag_3PO_4 (ref. 3) and Ag_2CO_3.[4] This is due to their high visible light absorption that yields an effective photocatalytic degradation of organic pollutants from aqueous media.[5,6] Nevertheless, their photo-activity efficiency depends on the anion nature since for instance, Ag-oxosalt photocatalytic performances increased in the order $Ag_3AsO_4 > Ag_3PO_4 > Ag_2CO_3 > Ag_2SeO_4 > Ag_2SO_4$.[7] However, this order seemed to be controversial in that a recent study reported that Ag_2CO_3 appeared more photoactive and photostable than Ag_3PO_4.[8] Likewise, this order depended on the nature of the pollutant.[8] Despite this, Ag_3PO_4, has been the most studied in photocatalysis with about 900 research papers dedicated to this compound compared to about 150 for Ag_2CO_3 in the same period.[9] This highest interest for Ag_3PO_4 was likely due to its better thermal stability and higher photoactivity, which could be further enhanced by doping.

In this context, several studies reported Ag_3PO_4 doping with Ni^{2+} (ref. 10) or Cu^{2+} (ref. 11) cations, and SO_4^{2-} (ref. 12) or CO_3^{2-} anions.[13] Considering anion doping, it is difficult to claim the achievement of the doping of an Ag-oxosalt by a polyatomic anion since the authors do not clearly explain how 5 ions (S^{6+} and O^{2-}) issued for instance from SO_4^{2-} group were distributed in the crystalline matrix. A more generic term than doping could be activation or treatment of the photocatalyst. For example, a so-called doping by SO_4^{2-} could be similar to a doping by sulfur. Anyway, in the particular case of Ag_3PO_4 doping by SO_4^{2-}, it was suggested that an electronic transfer occurred between SO_4^{2-} and PO_4^{3-}, more precisely from atomic orbitals S $3s^23p^4$ to P $3s^23p^3$.[12] The photocatalyst Ag_2CO_3 crystallizes in a monoclinic structure significantly different than the cubic structure of Ag_3PO_4. In addition, it presents an optical band gap (≈ 2.4 eV) in the same order of magnitude as the silver phosphate and thus is photoactive under visible light irradiation.[4] Nonetheless, in comparison with Ag_3PO_4, it was less studied as photocatalyst, probably due to the fact that, as other silver oxosalts, it exhibited drawbacks related for instance to a lower transfer rate of charge carriers[14] and a higher sensitivity to photocorrosion.[15] By contrast with Ag_3PO_4, fewer strategies have been explored to improve the performance of Ag_2CO_3.

To overcome these issues, several routes have been proposed such as heterojunctions between Ag_2CO_3 and another semi-conductor, which can promote high separation of the photo-generated electrons–holes pairs. This approach has been extended to nanocomposites with metal nanoparticles as Ag to produce Schottky junctions. For this purpose, beneficial heterojunctions were reported for TiO_2/Ag_2CO_3,[16] ZnO/Ag_2CO_3,[17] Ag/Ag_2CO_3,[18] Ag_2O/Ag_2CO_3,[19] Ag_3PO_4/Ag_2CO_3 (ref. 20) and AgX (X = Cl, I and Br)/Ag_2CO_3.[21] Another way[22] reported the effect of

[a]IMED-Lab, Sciences and Technologies Faculty, Cadi Ayyad University, Avenue Abdelkrim Khattabi, Box 549, Marrakech, Morocco

[b]CIRIMAT, Université de Toulouse, CNRS-UPS-INP, ENSIACET, 4 allée Emile Monso, BP 44362, 31030 Toulouse, cedex 4, France. E-mail: b.rhouta@uca.ma

varying types and ratios of solvents upon the synthesis in tunning the size and morphology of Ag_2CO_3 and consequently improving its photocatalytic activity and photostability. In another route, it was reported that the immobilization of Ag_2CO_3 particles on supports with a large specific surface area such as graphene oxide,[23] C_3N_4 (ref. 24–26) and some clay minerals like palygorskite[27] was also a promising way. Surprisingly, in contrast to Ag_3PO_4, anionic modification of Ag_2CO_3 was not investigated. In particular, the route of modification by SO_4^{2-} was not yet reported for improving photocatalytic properties of Ag_2CO_3.

Since both Ag-oxosalts differ in their crystallographic structure and anion nature (size, charge, composition), the response of these photocatalysts to a strategy will not necessarily be the same from one to another. The fact that SO_4^{2-} presents an ionic radius of the same order of magnitude than CO_3 (ref. 2–28) should facilitate bulk modification of Ag_2CO_3. However, the differences both in crystallographic structure between Ag_2CO_3 and Ag_3PO_4, and in charge transfer expected between the modifying anion (SO_4^{2-}) and crystal lattice anion (CO_3^{2-}), does not allow to think that the effects of the modification by SO_4^{2-} should be similar for Ag_2CO_3 and Ag_3PO_4.[12] These differences increase the interest of exploring Ag_2CO_3 modification with SO_4^{2-} as a route to enhance photocatalytic properties and paving a new way to improve the stability against photocorrosion for practical applications.

In this paper, the photocatalytic performances were assessed (i) by measuring the degradation rate of a model pollutant under visible light irradiation (kinetic data), (ii) by analyzing the extent of mineralization (TOC analysis), (iii) by determining the nature of photogenerated oxidizing species responsible of the dye photocatalytic degradation through scavenger experiments (resulting in hypothesis on the reaction mechanism) and (iv) by studying the photo-stability in reuse experiments.

2 Experimental

2.1 Synthesis of the photocatalysts

All reagents were of analytical grade and used without further purification. Pure Ag_2CO_3 was synthesized according to a method previously published.[4,27] For Ag_2CO_3 treatment with SO_4^{2-}, the method was adapted from that already reported for sulfate-doped Ag_3PO_4.[12] In a typical procedure, 20 mL of a translucent mixture of $AgNO_3$ (0.272 M) and Na_2SO_4 (0.0125 M) was prepared at room temperature in distilled water and stirred during 10 min for homogenization. Then 40 mL of Na_2CO_3 (0.068 M) was added dropwise under continuous stirring. The formed precipitate (*i.e.* SO_4^{2-}-modified Ag_2CO_3) was collected by centrifugation, washed with distilled water and ethanol three times to remove reaction byproducts mainly $NaNO_3$, Na_2SO_4 and traces of remaining reactants. The samples were dried at 60 °C overnight, then stored in the dark at room temperature before being used. With these synthesis conditions, the theoretical SO_4^{2-} content of the photocatalyst cannot exceed 9 at% since this was the value of the SO_4^{2-}/CO_3^{2-} anion ratio used.

2.2 Characterization techniques

The phase identification was carried out by X-ray diffraction (D8 Advance Diffractometer Bruker) with Cu Kα radiation source. The scanning was performed at room temperature in the 2θ range from 5° to 70° with a step size of 0.05° for 1 s. Infrared spectroscopy analysis was performed on a pellet of KBr–photocatalyst mixture (≈ 1 wt%) using a PerkinElmer FTIR in the range 400–4000 cm^{-1}. The SEM microscopy observations were performed using a scanning electron microscope VEGATESCAN3 coupled with an EDAX analyzer for elemental analysis. UV-vis Diffuse Reflectance Spectra (DRS) were recorded with respect to PTFE as standard using a Cary 5000 UV-vis-NIR spectrophotometer for wavelengths ranging from 200 to 800 nm. The zeta potential of the synthesized Ag-oxosalt powders was measured at room temperature in an aqueous suspension using a Zetasizer apparatus from Nano ZS, Malvern instruments.

2.3 Photocatalytic tests under visible light

The photocatalytic activity was evaluated by recording the temporal variation of Orange G (OG) concentration during its degradation under visible light irradiation in presence of the photocatalyst. OG is an anionic azo dye with the formula $C_{16}H_{10}N_2Na_2O_7S_2$. It was selected as model pollutant because it is frequently used as dye in textile industry, and it does not undergo photolysis under the conditions of this test. The visible light irradiation was provided by 4 light color/840 lamps (13 W each) coupled with a UV cut-off filter ($\lambda < 400$ nm). Practically, 25 mg of the photocatalyst was dispersed into a quartz photoreactor containing 25 mL of OG (10^{-5} M) aqueous solution. It should be noted that such conditions were the same as the ones already established by Lakbita *et al.*[27] to be optimal for the study of photocatalytic performances under visible light of Ag_2CO_3 supported palygorskite clay mineral in a similar slurry reactor. Afterwards, the suspension was stirred in the dark for 30 min to achieve adsorption–desorption equilibrium before to start the photocatalytic test by switching on the lamps. At regular time intervals, aliquots were picked up, centrifuged and OG concentration in supernatant was determined using UV-vis spectrophotometer from the intensity of the OG absorption band in the range 470–500 nm. It should be noted that a calibration curve in the Beer–Lambert linearity domain was checked beforehand in the low concentration range (10^{-7}–10^{-4} M) that includes the test value (10^{-5} M). The experimental data reported here were the average of 3 photocatalytic tests and an error bar represented the dispersion of data.

To check if the photocatalytic degradation of OG organic dye pollutant led to its partial or total mineralization, the Total Organic Carbon (TOC) corresponding to remaining organic dye plus possibly organic byproducts was determined after the test using a TOC analyzer (TOC-L CPH/CPN, Shimadzu). For this purpose, after the test, photocatalyst dispersion was centrifuged at 12 000 rpm during 5 min and the resulting supernatant was analyzed.

To further investigate the photocatalytic mechanism that would ensure the OG photocatalytic degradation, isopropanol

(IPA) was utilized to quench hydroxyl radicals ($^{\bullet}$OH),[12] tri-chloromethane (TCM) served as scavenger of superoxide radical anions ($^{\bullet}O_2^-$),[29] indigo carmine (IC) used to trap the ozonide radicals ($^{\bullet}O_3^-$)[8] and ethylenediamine tetra-acetic acid disodium (EDTA) was used as a hole (h^+) scavenger.[30] Before adding Ag_2CO_3 or SO_4^{2-}-Ag_2CO_3 powders and running photocatalysis experiment, 1 mM of each scavenger was added to the OG dye solution.[31]

3 Results and discussion

3.1 Bulk modification of Ag_2CO_3 by SO_4^{2-}

As shown in Fig. 1, XRD patterns recorded on unmodified and SO_4^{2-} modified Ag_2CO_3 appeared quite similar with several diffraction peaks amongst which the ones at 2θ around 18.32° ($d_{100} = 4.85$ Å), 18.54° ($d_{020} = 4.78$ Å), 20.5° ($d_{110} = 4.32$ Å), 32.74° ($d_{\bar{1}01} = 2.73$ Å), 33.81° ($d_{130} = 2.65$ Å), 37.07° ($d_{200} = 2.42$ Å) and 39.60° ($d_{031} = 2.27$ Å). These peaks were indexed on the basis of the stable monoclinic Ag_2CO_3 phase (ICDD file no. 01-070-2184). This result confirmed that the Ag_2CO_3 treatment by SO_4^{2-} had no effect on the crystallographic structure of the silver carbonate that remained monoclinic while several poly-types exist.[27] Furthermore, the non-appearance of additional peaks in the SO_4^{2-} modified Ag_2CO_3 pattern denoted the absence of any crystallized secondary phases as byproducts from the base reactions (*e.g.* Ag_2SO_4) or from side decomposition reactions (*e.g.* Ag_2O, Ag). Regarding Ag_2SO_4, the corresponding main XRD peaks, expected at 31.13° (311) and 28.08° (040), were not present (Fig. 1). This is consistent with the fact that it is water-soluble and was therefore washed away from the final photocatalyst powder (see Section 2.1).

Further detailed analysis of the diffractograms interestingly revealed a slight shift of the peaks towards smaller 2θ angles. Indeed, in the 2θ region between 32.0° and 34.5°, ($\bar{1}01$) and (130) peaks were observed respectively at 32.74° and 33.81° for pure Ag_2CO_3 while they appeared at 32.64° and 33.69° for SO_4^{2-} modified Ag_2CO_3 (Fig. 1b). The values of a, b, and c lattice

parameters and β angle of unmodified- and SO_4^{2-} modified Ag_2CO_3 samples, were calculated from all the XRD peaks, using the Unit Cell software.[32] They were reported in Table S1 (ESI).† They revealed an increase of the lattice parameters for SO_4^{2-}-modified Ag_2CO_3 with respect to unmodified Ag_2CO_3 corresponding to a volume expansion of the unit cell of *ca.* 1.0%, which was certainly due to the higher ionic radius of SO_4^{2-} (0.218 nm) compared to the one of CO_3^{2-} (0.189 nm).[28] This finding ascertained that CO_3^{2-} anions in the crystal lattice were substituted by modifying SO_4^{2-} anions larger by 15% and hence confirmed the achievement of a bulk modification of Ag_2CO_3 by sulfate anions. This ruled out a simple surface functionalization by SO_4^{2-} anions grafted on Ag_2CO_3 particles, which should not induce an expansion of the crystal lattice.

To complete the crystallographic analysis, the two photo-catalysts were characterized by FTIR spectroscopy. In addition to the presence of H_2O molecules that was revealed by absorption bands around 3200 and 1650 cm^{-1}, both FTIR spectra exhibited characteristic absorption bands of Ag_2CO_3 (Fig. 2). The two intense bands at 1442 and 1377 cm^{-1}, as well as those at 879 and 697 cm^{-1} may be assigned to the distinctive vibrations of the planar CO_3^{2-} groups, *i.e.* deformation and stretching, respectively.[33] Additional bands were exclusively detected in SO_4^{2-}-modified Ag_2CO_3 sample with bands at 1113, 1056, and 606 cm^{-1} attributed to the stretching mode of S–O and O–S–O bonds in SO_4^{2-} tetrahedra, as reported for Ag_2SO_4 elsewhere.[34] Except the bands of CO_3^{2-} and SO_4^{2-} anions (and H_2O traces), no other absorption band was observed in the sulfate modified Ag_2CO_3 photocatalyst. This result further supported the beforehand mentioned statement issued from XRD analysis according to which on one hand a bulk modification of Ag_2CO_3 with SO_4^{2-} anions was successfully achieved rather than a sulfate anion grafting on the surface of Ag_2CO_3 particles and on the other hand the absence of secondary phases formation.

SEM analyses showed that pure Ag_2CO_3 and SO_4^{2-}-Ag_2CO_3 samples exhibited the same microstructure with micron-size
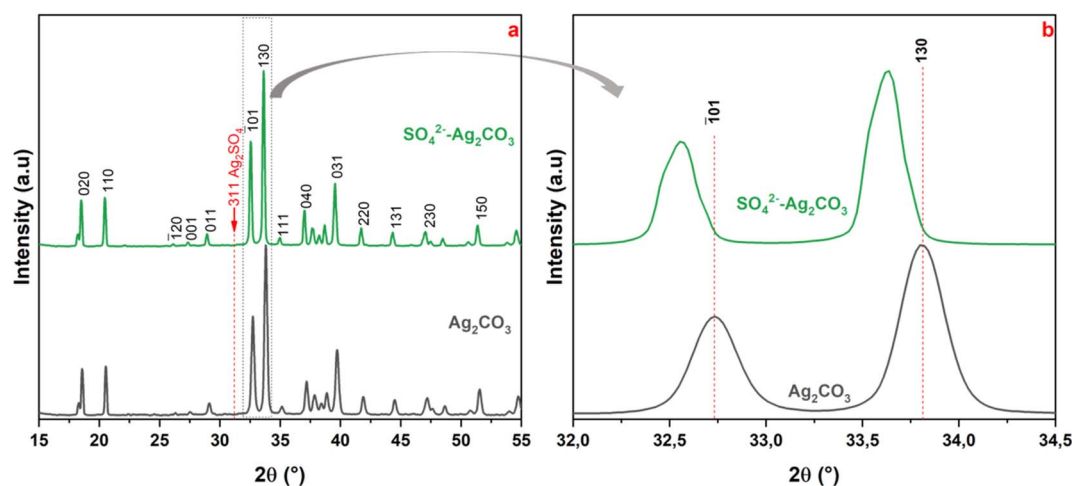

Fig. 1 X-ray diffraction patterns of pure Ag_2CO_3 and SO_4^{2-} modified Ag_2CO_3 (left) and zoom in the 32.0°–34.5° angular region corresponding to ($\bar{1}01$) and (130) reflection planes of both Ag_2CO_3 and SO_4^{2-}-Ag_2CO_3 (right).
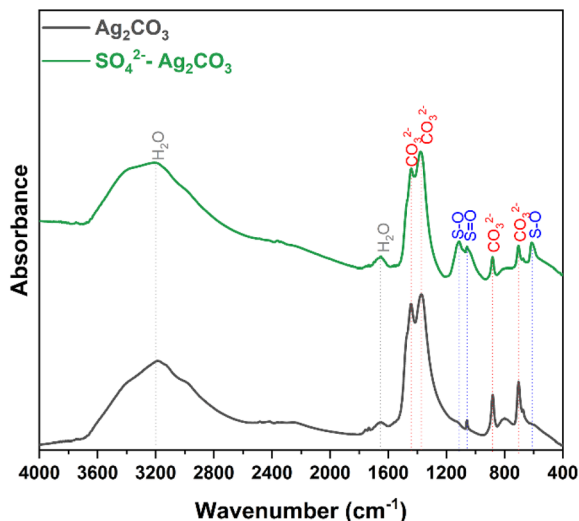
Fig. 2 FTIR spectra of pure Ag_2CO_3 (bottom) and SO_4^{2-} modified Ag_2CO_3 (top). The absorption bands were assigned according to literature data of carbonates and sulfates including Ag_2CO_3[33] and Ag_2SO_4.[34]

and monodisperse particles with pretty similar polyhedral shapes (Fig. 3). They appeared well crystallized, in the form of facetted rhombohedra with an average size of 0.3 μm according to the Dynamic Light Scattering (DLS) particle size distribution analysis (Fig. S1†). This microstructure was similar to that previously reported for silver carbonate synthesized by the same method.[27] Therefore, SO_4^{2-}-modification did not change the

microstructure of Ag_2CO_3 particles (Fig. 2). This should be consistent with the incorporation into the Ag_2CO_3 crystal lattice of only a very small amount of SO_4^{2-} anions. This assumption was further supported by EDS analysis showing the SO_4^{2-}-Ag_2CO_3 sample was mainly composed of Ag, C, O. Very small peak, corresponding to sulfur, was detected in the energy range (Fig. 3d). Moreover, the SEM-EDS elemental mapping of the SO_4^{2-}-Ag_2CO_3 powder spread on the sample holder did not reveal any evidence for S-rich regions, which additionally confirmed the absence of secondary phase such as Ag_2SO_4 (Fig. 3). Thus, the S amount in SO_4^{2-}-Ag_2CO_3 sample was estimated to be around 1.8 atomic% fraction, which is way lower than the 9% allowed by the initial proportion of reagents and confirms the Ag_2CO_3 modification with SO_4^{2-}.

UV-vis diffuse reflectance spectra recorded on pure Ag_2CO_3 and SO_4^{2-} modified Ag_2CO_3 samples did not reveal significative differences. For both the samples, they displayed a high and sharp absorption below 500 nm, in the visible light range, denoting as expected their wide band gap semiconductor characters (Fig. 4a). In both the cases, there was no evidence of absorption band above 500 nm that could be due to plasmonic effect induced by Ag nanoparticles as reported elsewhere.[35] The recorded UV-vis spectra herein were in good agreement with those previously reported for monoclinic Ag_2CO_3.[4,8,15] The absorption edges, corresponding to the intersection of the extrapolation of the linear part of the absorption curve with the wavelength axis, were determined to be around 509 nm (2.44 eV) and 533 nm (2.33 eV) for pure Ag_2CO_3 and SO_4^{2-}-modified Ag_2CO_3 samples, respectively (Fig. 4a).
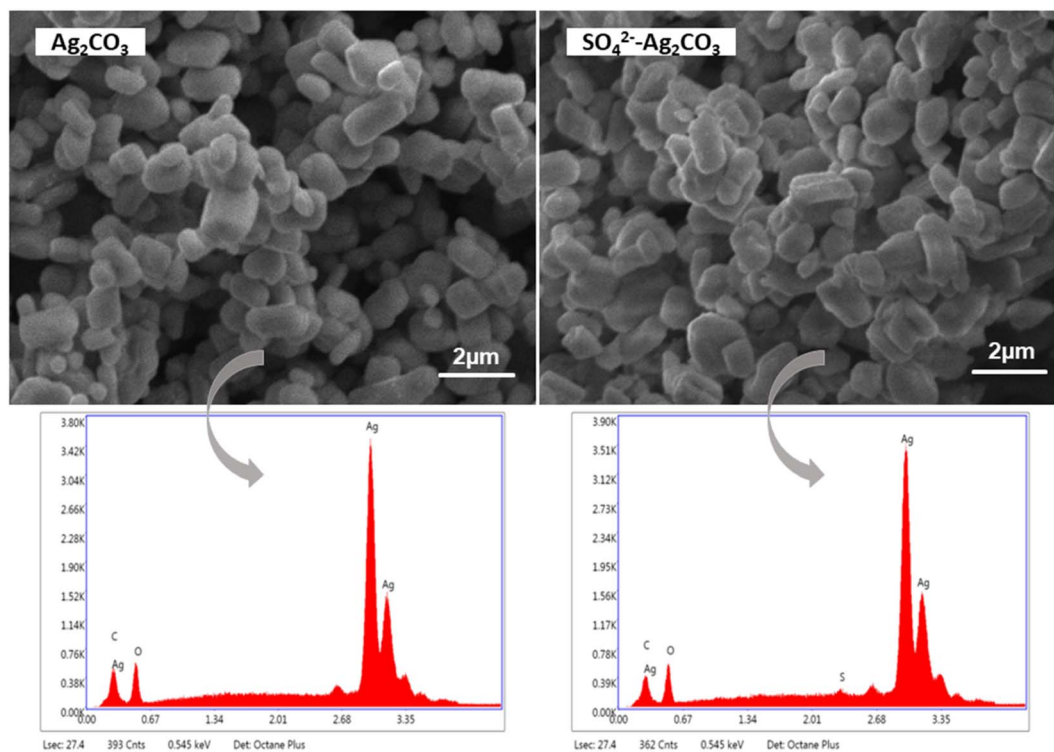

Fig. 3 SEM micrographs of pure Ag_2CO_3 (left) and SO_4^{2-} modified Ag_2CO_3 (right), and the EDS spectra corresponding to each image.
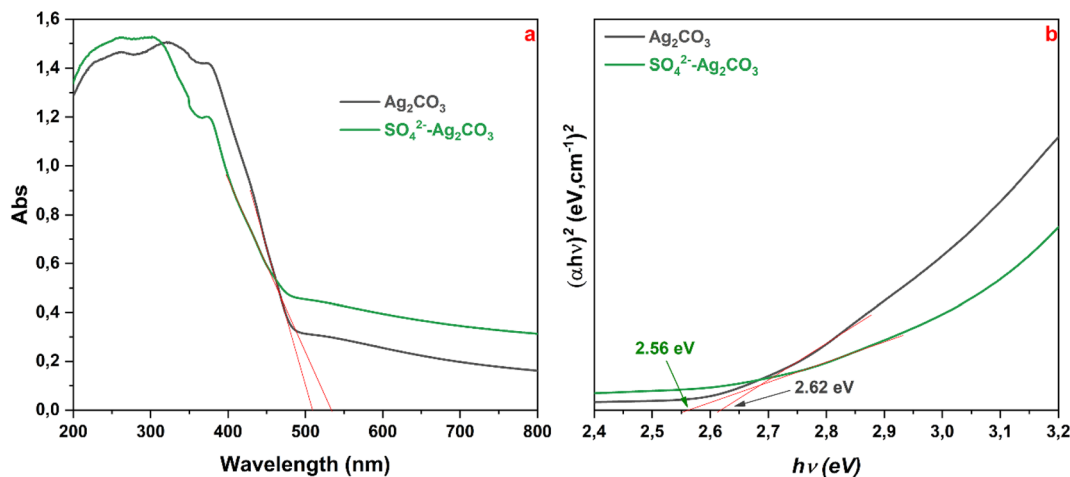
Fig. 4 UV-vis DRS spectra of Ag_2CO_3 and SO_4^{2-}-Ag_2CO_3 samples (a), and corresponding plot $(\alpha h\nu)^2$ vs. energy $h\nu$ (b). Red straight lines are extrapolations to determine optical gap (absorption edge) from (a) and the Tauc band gap energy from (b).

As both the Ag_2CO_3-based compounds are indirect semiconductors according to previously reported studies,[4,7,8] the corresponding band gap energies (E_g) determined by the Tauc method[4] were found to be about 2.62 and 2.56 eV, for unmodified and SO_4^{2-} modified Ag_2CO_3 respectively (Fig. 4b). These E_g values were consistent with those of Ag_2CO_3 which were reported over a fairly wide range from 2.30 eV[15] to 2.62 eV[20] depending on the synthesis method, the crystallographic structure, the microstructure and purity (Table S2 in ESI†). In this respect, as beforehand evidenced that the treatment by SO_4^{2-} did change neither the structure (Fig. 1) nor the microstructure of Ag_2CO_3, the slight decrease of E_g ($\approx 2.3\%$) between both the band gap energies may result from the anionic modification effect. This SO_4^{2-} effect contrasted with that exerted by Ag_3PO_4 doping by SO_4^{2-} yielding rather to a slight increase of E_g as reported elsewhere.[12] Therefore, SO_4^{2-}-modified Ag_2CO_3 photocatalyst exhibited a slightly better absorption of the photons in the visible range. This means that, as more discussed below, more photo-generated electrons (e^-) were transferred from the valence band (VB) to the conduction band (CB), leaving more holes (h^+) in the VB that will be capable of oxidizing more organic species in primary reactions.

Furthermore, the valence band position (E_{VB}) and the conduction band position (E_{CB}) of SO_4^{2-}-Ag_2CO_3 can be computed through the Mulliken electronegativity empirical equations:[15]

$$E_{VB} = \chi - E_0 + 0.5E_g \qquad (1)$$

$$E_{CB} = E_{VB} - E_g \qquad (2)$$

where χ is the semiconductor absolute electronegativity (6.023 eV for Ag_2CO_3 (ref. 8 and 15) and E_0 is the free electron energy on the hydrogen scale, otherwise the Fermi level of NHE (Normal Hydrogen Electrode) with respect of the vacuum level (ca. 4.5 eV). E_{VB} and E_{CB} are the VB and CB edge potentials respectively, and E_g is the band gap of the semiconductor. The E_{VB} and E_{CB} values hence deduced for SO_4^{2-}-modified Ag_2CO_3

were +2.80 and +0.24 eV, respectively. For pure Ag_2CO_3 the values found were +2.83 and +0.21 eV respectively. These values were in agreement with literature data for Ag_2CO_3 based compounds (Table S2†).

3.2 Visible-light photocatalytic properties

The variation of OG dye concentration *versus* irradiation time under visible light in presence of pure Ag_2CO_3 and SO_4^{2-}-Ag_2CO_3 photocatalysts was reported in Fig. 5. It is worth noting that keeping beforehand in the dark during 30 min the dispersion of the two photocatalysts in OG aqueous solution did not reveal OG adsorption onto the surface of the two photocatalysts due to electrostatic repulsions between anionic OG dye molecules and negatively charged surfaces of the photocatalysts. This was confirmed by the zeta potentials measured to be -23 mV for pure Ag_2CO_3 and -27 mV for SO_4^{2-}-Ag_2CO_3, which was consistent with that reported elsewhere (-36 mV) for the pure silver carbonate.[7] Furthermore, the concentration of OG solution free from photocatalyst appeared not decreasing during the whole duration of its exposure to visible light. This proved that OG dye did not undergo photolysis (Fig. 5a).

In the presence of pure Ag_2CO_3, OG concentration considerably decreased during the first 20 minutes of irradiation to reach an OG degradation plateau after a removal of ca. 60% (Fig. 5a) beyond which no more dye photocatalytic degradation occurred. This striking behavior could be ascribed either to (i) surface Ag_2CO_3 poisoning by byproducts issued from photocatalytic reactions, or (ii) to photocorrosion of the photocatalyst induced by premature Ag_2CO_3 decomposition under light irradiation. The second assumption seemed to be of minor impact since the catalyst has been found still active in reuse experiments as further discussed in the Section 3.3. The observation of photocatalytic degradation threshold has already been reported upon assays involving pure Ag_2CO_3 against Methyl Orange (MO) anionic dye,[7,8] and Rhodamine B (RhB)[7,8,18] and Methylene Blue (MB)[7] cationic dyes despite their electrostatic attraction by negatively Ag_2CO_3 surfaces. In contrast, the most
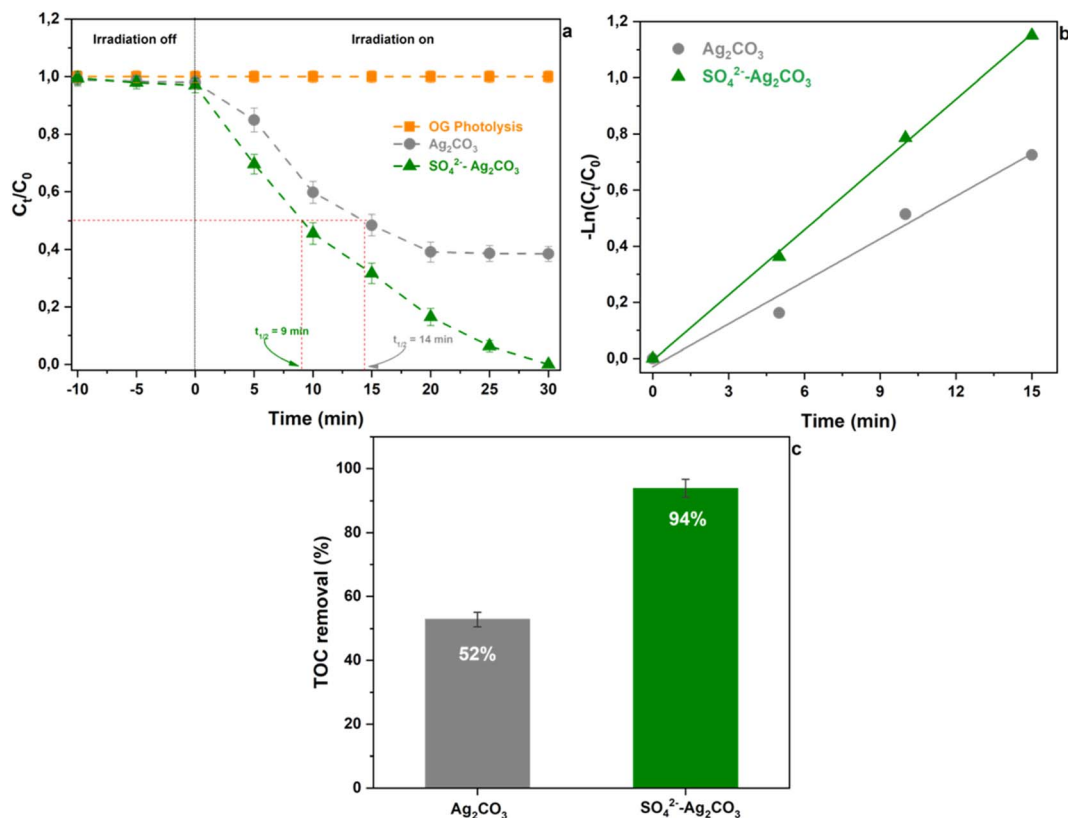
Fig. 5 Variation of the relative OG concentration *vs.* irradiation time over Ag_2CO_3 and SO_4^{2-}-Ag_2CO_3 (a). Plots of $-\ln(C_t/C_0)$ *vs.* irradiation time for the two photocatalysts (b). Proportion of Total Organic Carbon (TOC) removal analyzed upon OG photocatalytic degradation under visible light irradiation during 30 min (c). The errors bars in (a) and (c) correspond to the data dispersion from 2 experiments.

salient result from the use of SO_4^{2-}-Ag_2CO_3 photocatalyst was that the relative OG concentration continuously decreased during the photocatalytic test to reach remarkably a total removal of the dye pollutant within 30 min (Fig. 5a). This denoted its relative better photostability, *i.e.* a higher resistance to both surface poisoning and photo-corrosion issues as below evidenced in Section 3.3.

For both the pristine photocatalyst and SO_4^{2-}-modified photocatalysts, OG dye photocatalytic degradation obeyed a pseudo first-order kinetics during approximately the first 15 min of visible light illumination. The rate constant assessed in this time range was about 5.1×10^{-2} min^{-1} for pure Ag_2CO_3 and 7.8×10^{-2} min^{-1} for SO_4^{2-}-Ag_2CO_3 (Fig. 5b). This result denoted that the photocatalytic activity of the SO_4^{2-}-modified sample was *ca.* 1.5 times faster than that of pure Ag_2CO_3.

The mineralization of OG, *i.e.* its ability to be converted into H_2O and CO_2 upon photocatalytic degradation, was also investigated. Fig. 5c depicted the total organic carbon (TOC) removal analyzed in the supernatant aqueous solution after a 30 min photocatalytic test using each photocatalyst. In presence of Ag_2CO_3, only around 52% of the TOC was removed, otherwise the proportion of OG and eventually its organic byproducts originated from photocatalytic reactions which was able to be mineralized. It should be noted that this OG amount was of the same magnitude order than that ($\approx 60\%$) previously assessed by

in situ UV-VIS spectrophotometry during the photocatalyst test. Nevertheless, it is worth noting that upon the use of SO_4^{2-}-Ag_2CO_3, almost 94% of the TOC was removed, indicating a relatively huge mineralization of OG dye. Interestingly, it should be noted that this amount was fairly close to the 100% of OG photo-catalytically degraded assessed above by UV-VIS spectrophotometry.

3.3 Effect of SO_4^{2-} modification on Ag_2CO_3 stability

The above presented results highlighted that modification of Ag_2CO_3 by SO_4^{2-} could be an efficient route to enhance the photocatalytic activity under visible light with (i) a higher degradation rate, (ii) an almost complete decomposition of the organic pollutant and (iii) a high efficiency of mineralization of the OG dye. However, the effect of SO_4^{2-} anions on both the stability of the photocatalyst and the photocatalytic oxidation mechanism needed to be investigated for further improvement and practical applications.

To investigate the behavior of pure and sulfate-modified Ag_2CO_3 photocatalysts towards photo-corrosion issue, cycling experiments were performed. Fig. 6a reported the relative variation of OG concentration *versus* irradiation time under visible light recorded in presence of both the photocatalysts during three successive runs of 30 min each one. As previously mentioned, when using pure Ag_2CO_3, the dye photocatalytic
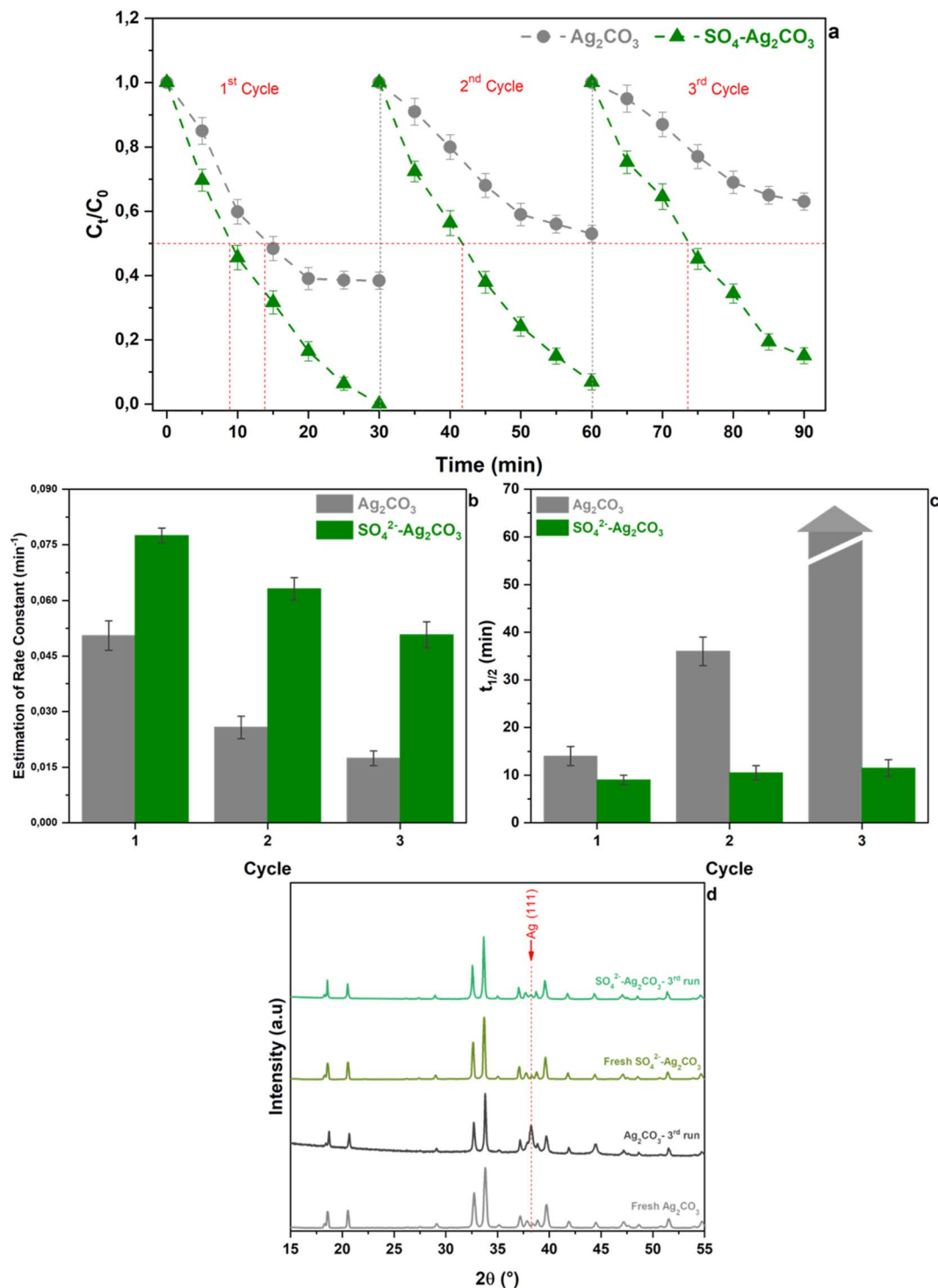
RSC Advances

Fig. 6 Cycling runs for OG photodegradation under visible light irradiation over pure Ag_2CO_3 and SO_4^{2-}-Ag_2CO_3 (a). Rate constant (b) and half-photodegradation time of OG ($t_{1/2}$) versus cycling of pure Ag_2CO_3 and SO_4^{2-}-Ag_2CO_3 photocatalysts (c). X-ray diffraction patterns of unmodified Ag_2CO_3 and SO_4^{2-} modified Ag_2CO_3 after the 3rd cycle (d). The errors bars in (a)–(c) correspond to the data dispersion from 2 experiments.

degradation curve reached a plateau after 20 min of irradiation in the 1st cycle and the same behavior tended to be exhibited during the 2nd and 3rd cycles. It should be noted that as the cycles number increased, the maximal amount of OG removed decreased from approximately 60% at the end of the 1st cycle, to

45 and 35% after the 2nd and 3rd ones respectively. Accordingly, the corresponding rate constants deduced over the first 15 minutes, labelled R_{15}, also rapidly decreased from 5.1×10^{-2} min^{-1} for the 1st cycle to 2.6×10^{-2} and 1.7×10^{-2} min^{-1} for the 2nd and 3rd ones, respectively (Fig. 6b). This steady

decline of rate constants corresponded to an efficiency loss with respect to the 1st cycle of 50 and 65% for the 2nd and 3rd ones respectively. These results ascertained the poor stability of pure Ag_2CO_3 in agreement with elsewhere reported studies.[8,15] The variation of the OG half-degradation time ($t_{1/2}$) versus cycling recorded upon the use of Ag_2CO_3 (Fig. 6) showed that $t_{1/2}$ of about 14 min for the 1st cycle strongly increased to 35 min for the 2nd one while it cannot be determined after 3 cycles since the total amount of OG removed did not exceed 35% (Fig. 6c). These results further supported previous deductions (Section 3.2) regarding the low stability and/or deactivation, by being sensitive to photo-corrosion and/or poisoning issues respectively, of the unmodified Ag_2CO_3.

By contrast, the OG concentration variation curves versus cycling, recorded in presence of SO_4^{2-}-Ag_2CO_3 photocatalyst, showed a continuous and very noticeable OG photocatalytic degradation versus irradiation time under visible light regardless the cycling run number (Fig. 6a). In fact, while OG dye was completely removed after 30 min during the 1st cycle, denoting 100% of removal efficiency, the efficiency remained greater than 90% and 80% over the same period upon the 2nd and the 3rd cycles, respectively. Likewise, the corresponding R_{15} rate constants slightly decreased from 7.8×10^{-2} min^{-1} after the 1st

cycle to 6.3×10^{-2} min^{-1} after the 2nd and to 5.1×10^{-2} min^{-1} after the 3rd cycle, which corresponded to a thorough efficiency loss of about 35% being slighter than that (65%) previously computed for pure Ag_2CO_3 (Fig. 6b). The better stability of SO_4^{2-}-Ag_2CO_3 photocatalyst was also illustrated throughout the assessment of $t_{1/2}$ values versus cycling. Fig. 6c revealed that $t_{1/2}$ remained quite of the same magnitude order around 10 min regardless the cycle run number. Furthermore, powder XRD carried out on unmodified Ag_2CO_3 sample, recovered after the 3rd cycle, revealed the appearance of a very intense peak ascribed to (111) metallic silver (Ag) (Fig. 6d). This observation denoted that bare Ag_2CO_3 underwent photo-corrosion issue. Nevertheless, it is worth noting that such Ag peak was very hardly observed in SO_4^{2-}-Ag_2CO_3 after the same run of photocatalysis test. The whole of these results concorded for proving that Ag_2CO_3 modification by SO_4^{2-} likely appeared to be an effective and efficient way to improve the resistance of Ag_2CO_3 against photo-corrosion as well as poisoning issues, and thus to enhance photocatalytic activity.

3.4 Photocatalytic mechanism

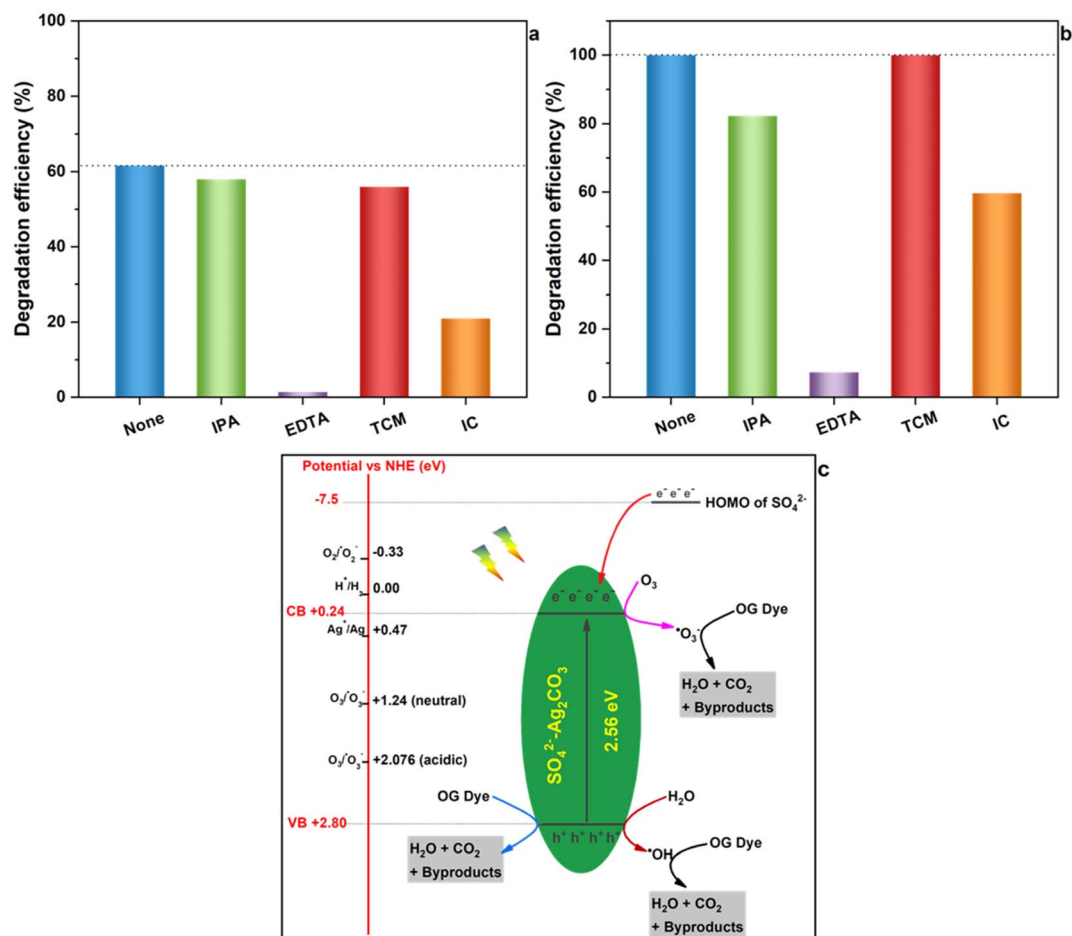In order to explore the photocatalytic mechanism of both Ag_2CO_3 and SO_4^{2-}-Ag_2CO_3 photocatalysts, reactive species

Fig. 7 Photocatalytic degradation of OG by Ag_2CO_3 (a) and SO_4^{2-}-Ag_2CO_3 (b) under visible light irradiation in the presence of scavengers: IPA, EDTA, TCM and IC. Schematic illustration of the plausible mechanism of OG degradation in presence of SO_4^{2-}-Ag_2CO_3 photocatalyst (c).

trapping experiments were performed to elucidate the main oxidants responsible of OG degradation under visible light irradiation, including hydroxyl radical ($^{\bullet}$OH), superoxide radicals ($^{\bullet}O_2^-$), ozonide radicals ($^{\bullet}O_3^-$) and photoinduced holes (h^+). The obtained results, gathered in Fig. 7(a) and (b), did not reveal significant differences in the behavior of both the investigated Ag_2CO_3 based photocatalysts towards the radicals trapping agents above-mentioned. Indeed, the addition of TCM, as $^{\bullet}O_2^-$ scavenger, had no noticeable effect on OG photocatalytic degradation since the efficiency almost remained constant in both the cases like before using the trapper. This likely stood for the noninvolvement of $^{\bullet}O_2^-$ in OG degradation. The use of IPA, as hydroxyl radical trapper, yielded a small decrease in the photocatalytic degradation efficiency of OG within 30 min from initially almost 62% and 100% to around 58% and 82% over unmodified and modified Ag_2CO_3 respectively. Hence, $^{\bullet}$OH radicals seemed to play a minor role in OG photocatalytic degradation. Nevertheless, it is noteworthy that using IC quencher of $^{\bullet}O_3^-$ provoked a relatively huge decrease of the OG degradation efficiency estimated at almost 40% in both the cases. This denoted that the contribution of $^{\bullet}O_3^-$ radicals in OG photocatalytic degradation may be substantial. The most salient effect was that of the addition of EDTA as h^+ trapper which thoroughly made both the Ag_2CO_3 based photocatalysts unactive towards the OG removal. This likely ascertained that photoinduced holes (h^+) was the major reactive species responsible of OG photocatalytic oxidation over both the investigated photocatalysts.

These results were further supported by the values of redox potentials of the top of valence band (VB) and the bottom of conduction band (CB) beforehand computed for both the Ag_2CO_3 based photocatalysts studied herein (Section 3.1) that were reported in Fig. 7c on which were also placed potentials of different reactive species in photocatalysis. In fact, the potential of photoelectrons on CB is too positive (0.24 eV) to be able to permit the reduction of dissolved O_2 in aqueous medium into $^{\bullet}O_2^-$ species whose potential is −0.33 eV. Therefore, $^{\bullet}O_2^-$ entities cannot come into play in the OG photocatalytic degradation over Ag_2CO_3 based photocatalysts, and must be excluded as also emphasized by W. Jiang *et al.*[8] This deduction was in contrast to results reported by several authors[4,34] proposing the involvement of $^{\bullet}O_2^-$ in the photodegradation of rhodamine B and/or Methylene Orange and/or Methylene Blue over silver carbonate although the potential of photoelectrons they estimated was 0.29 eV and 0.37 eV respectively, *i.e.* too positive with respect to the negative one characterizing $O_2/^{\bullet}O_2^-$ couple. Nevertheless, the ozone, able to be provided from dissolved oxygen upon solution illumination,[8] present an electrode potential in neutral and acidic medium of 1.24 eV and 2.076 eV respectively so that it can be reduced by photoelectrons generated herein (0.24 eV) to yield the formation of oxidative $^{\bullet}O_3^-$ radicals which assured OG photocatalytic degradation onto both the investigated photocatalysts. Furthermore, taking into account the strongly oxidative electrode potential of photo-holes (h^+) herein estimated of about 2.80 eV, these photoinduced entities assured direct OG degradation. Likewise, h^+ specie could also hardly oxidize H_2O to provide $^{\bullet}$OH radical

whose the potential is close to its own (2.8 eV). This denoted that a part of h^+ may indirectly participate through a minor amount of $^{\bullet}$OH radical in the OG photodegradation onto both the studied photocatalysts. In light of all these results, the OG photocatalytic degradation under visible light seemed to be achieved according to on the whole a similar mechanism illustrated in Fig. 7c onto unmodified and sulfate modified Ag_2CO_3. The plausible mechanism likely mainly implied photo-holes acting as latent oxidative entities along with to a relatively lesser extent $^{\bullet}O_3^-$ reactive radicals and finally a minor participation of $^{\bullet}$OH hydroxyl radicals. Nonetheless, in view of the so proposed mechanism, one can ask how Ag_2CO_3 modification by SO_4^{2-} improved photostability as well as photocatalytic efficiency beforehand evidenced (Section 3.2 and 3.3)?

One beneficial key role of SO_4^{2-} anions would be their ability to contribute with 32 valence electrons to the lattice of the sulfate-modified Ag_2CO_3 photocatalyst, instead of 24 electrons for CO_3^{2-} anions, providing therefore a surplus of 8 valence electrons. As reported by Bishop *et al.*,[36] the Highest Occupied Molecular Orbital (HOMO) of SO_4^{2-} is located at around −7.5 eV, so that sulfate electrons can be transferred to lower $AgCO_3$ conduction band. Thus, these excess electrons provided by SO_4^{2-} together with those photogenerated in $AgCO_3$ upon illumination can reduce more ozone to produce more $^{\bullet}O_3^-$ reactive entities which can act as additional reactive species as evidenced above by IC trapping experiments. Consequently, the OG photocatalytic degradation could speed up as proved by corresponding higher rate constant with respect to that of the pristine Ag_2CO_3 above-computed in Section 3.2.

Another possible key effect of SO_4^{2-} on the improvement of Ag_2CO_3 photostability, beforehand evidenced upon photocatalytic tests (Section 3.2) and cycling experiments (Section 3.3), may be its capacity of electrons transfer to Ag^+ higher than that permitted by CO_3^{2-}. In fact, as widely reported, primary mechanism of photocorrosion of pure Ag_2CO_3 could be attributed to the reduction of Ag^+ cations, issued from Ag_2CO_3 solubilizing, by photoinduced e^-, which produced metallic Ag and, over time, a progressive Ag_2CO_3 depletion into Ag cations resulting at the end in the photocatalyst degradation.[2,4,15] Considering an isolated Ag^+–anion interaction, the fractional number of electrons transferred from the anion to Ag^+ cation can be estimated, according to the Pearson model[37] (details reported in the ESI†), to be about 0.29 and 0.21 for SO_4^{2-} and CO_3^{2-} respectively. This indicated that an interaction of SO_4^{2-} with Ag^+ cation was 38% greater than that of CO_3^{2-}. Such an effect can contribute to improve the stability of the photocatalyst because Ag^+ would be less reactive towards photoelectrons to form metal Ag, hence yielding photocorrosion issue to get mitigated.

4   Conclusion

Ag_2CO_3 modification with sulfate was achieved according to a simple precipitation method. This was confirmed by XRD that revealed a volume expansion of the monoclinic Ag_2CO_3 unit cell due to the substitution of CO_3^{2-} groups by the larger SO_4^{2-} anions. This was hence consistent with a bulk modification

rather than a simple surface grafting of SO_4^{2-} ions on Ag_2CO_3 particles. However, Ag_2CO_3 modification with SO_4^{2-} did not significantly affect the Ag_2CO_3 band gap. The evaluation of the photocatalytic degradation of OG dye under visible light revealed that the sulfate modified Ag_2CO_3 was more active than bare Ag_2CO_3 leading to the achievement of a quasi-total mineralization within 30 min of irradiation. In addition, evidence for poisoning and/or photocorrosion issues observed for pure Ag_2CO_3 did not occur for the modified photocatalyst. The active species trapping experiments revealed that the OG photocatalytic degradation seemed to be assured over both the photocatalysts by photoinduced holes (h^+) along with $\cdot O_3^-$ radicals, while $\cdot OH$ radicals would play a minor role. Improvements allowed by Ag_2CO_3 modification by SO_4^{2-}, in terms of increase of photocatalytic rate and enhancement of Ag_2CO_3 stability, could be due to valence electrons added to photoinduced electrons, as a result of their transfer from SO_4^{2-} HOMO to Ag_2CO_3 conduction band, which may together assure the formation of much active $\cdot O_3^-$ radicals entities. This proposed mechanism ought to be further validated by using more sophisticated characterization technique such as ESR and PL analyses and DFT calculations. On the whole, in view of the simple synthesis route of SO_4^{2-} modified Ag_2CO_3 photocatalyst and its promising performances, in term of enhancement of photoactivity and photostability under visible light at laboratory scale, this study should be carried on by evaluating its photocatalytic properties in an outdoor solar pilot. This will increase its prospect of application in the field of tertiary treatment of wastewater.

Conflicts of interest

There are no conflicts of interest to declare.

Acknowledgements

References

1 Y. Wang, N. Bi, H. Zhang, W. Tian, T. Zhang, P. Wu and W. Jiang, *Colloids Surf., A*, 2020, **585**, 124105.

2 Y. Wang, H. Liu, B. Wu, T. Zhou, J. Wang, J. Zhou, S. Li, F. Cao and G. Qin, *J. Alloys Compd.*, 2019, **776**, 948–953.

3 U. Sulaeman, F. Febiyanto, S. Yin and T. Sato, *Catal. Commun.*, 2016, **85**, 22–25.

4 H. Dong, G. Chen, J. Sun, C. Li, Y. Yu and D. Chen, *Appl. Catal., B*, 2013, **134–135**, 46–54.

5 G. Li, Y. Wang and L. Mao, *RSC Adv.*, 2014, **4**, 53649–53661.

6 J. Li, W. Fang, C. Yu, W. Zhou, L. zhu and Y. Xie, *Appl. Surf. Sci.*, 2015, **358**, 46–56.

7 X. Jin, I. Y. Kim, Y. K. Jo, J. L. Bettis Jr, H.-J. Koo, M.-H. Whangbo and S.-J. Hwang, *J. Phys. Chem. C*, 2013, **117**, 26509–26516.

8 W. Jiang, Y. Zeng, X. Wang, X. Yue, S. Yuan, H. Lu and B. Liang, *Photochem. Photobiol.*, 2015, **91**, 1315–1323.

9 *Document search – Web of Science Core Collection*, https://www.webofscience.com/wos/woscc/basic-search, (accessed November 9, 2022).

10 L. Song, Z. Chen, T. Li and S. Zhang, *Mater. Chem. Phys.*, 2017, **186**, 271–279.

11 H. El Masaoudi, I. Benabdallah, B. Jaber and M. Benaissa, *Chem. Phys.*, 2021, **545**, 111133.

12 W. Cao, Z. Gui, L. Chen, X. Zhu and Z. Qi, *Appl. Catal., B*, 2017, **200**, 681–689.

13 J. Luo, Y. Luo, Q. Li, J. Yao, G. Duan and X. Liu, *Colloids Surf., A*, 2017, **535**, 89–95.

14 H. Wang, J. Li, P. Huo, Y. Yan and Q. Guan, *Appl. Surf. Sci.*, 2016, **366**, 1–8.

15 G. Dai, J. Yu and G. Liu, *J. Phys. Chem. C*, 2012, **116**, 15519–15524.

16 Y. Wang, P. Ren, C. Feng, X. Zheng, Z. Wang and D. Li, *Mater. Lett.*, 2014, **115**, 85–88.

17 Z. Xiang, J. Zhong, S. Huang, J. Li, J. Chen, T. Wang, M. Li and P. Wang, *Mater. Sci. Semicond. Process.*, 2016, **52**, 62–67.

18 N. Yu, R. Dong, J. Liu, K. Huang and B. Geng, *RSC Adv.*, 2016, **6**, 103938–103943.

19 W.-K. Jo, S. Kumar, P. Yadav and S. Tonda, *Appl. Surf. Sci.*, 2018, **445**, 555–562.

20 W. Fa, P. Wang, B. Yue, F. Yang, D. Li and Z. Zheng, *Chin. J. Catal.*, 2015, **36**, 2186–2193.

21 J. Dostanić, D. Lončarević, V. Đorđević, S. P. Ahrenkiel and J. M. Nedeljković, *J. Photochem. Photobiol., A*, 2017, **336**, 1–7.

22 X. Yang, R. Li, Y. Wang, K. Wu, S. Chang and H. Tang, *Ceram. Int.*, 2016, **42**, 13411–13420.

23 C. Dong, K.-L. Wu, X.-W. Wei, X.-Z. Li, L. Liu, T.-H. Ding, J. Wang and Y. Ye, *CrystEngComm*, 2013, **16**, 730–736.

24 N. Tian, H. Huang, Y. He, Y. Guo and Y. Zhang, *Colloids Surf., A*, 2015, **467**, 188–194.

25 C. Feng, L. Tang, Y. Deng, J. Wang, J. Luo, Y. Liu, X. Ouyang, H. Yang, J. Yu and J. Wang, *Adv. Funct. Mater.*, 2020, **30**, 2001922.

26 C. Feng, Z.-P. Wu, K.-W. Huang, J. Ye and H. Zhang, *Adv. Mater.*, 2022, **34**, 2200180.

27 O. Lakbita, B. Rhouta, F. Maury, F. Senocq, M. Amjoud and L. Daoudi, *Appl. Surf. Sci.*, 2019, **464**, 205–211.

28 M. C. Simoes, K. J. Hughes, D. B. Ingham, L. Ma and M. Pourkashanian, *Inorg. Chem.*, 2017, **56**, 7566–7573.

29 A. Bouziani, M. Yahya, Y. Naciri, A. Hsini, M. A. Khan, M. Sillanpää and G. Celik, *Surf. Interfaces*, 2022, **34**, 102328.

30 K. Perumal, S. Shanavas, T. Ahamad, A. Karthigeyan and P. Murugakoothan, *J. Environ. Sci.*, 2023, **125**, 47–60.

31 X. Bu, C. Chen, X. Zhao, Q. Huang, X. Liao, H. Fan, P. Wang, H. Hu, Y. Zhang and Z. Huang, *Appl. Surf. Sci.*, 2022, **588**, 152887.

32 T. J. B. Holland and S. A. T. Redfern, *Mineral. Mag.*, 1997, **61**, 65–77.

33 H. Zeng, Z. Yu, L. Shao, X. Li, M. Zhu, Y. Liu, X. Feng and X. Zhu, *Desalination*, 2020, **491**, 114558.

34 E. Tomaszewicz, M. Kurzawa and L. Wachowski, *J. Mater. Sci. Lett.*, 2002, **21**, 547–549.

35 M. Rehan, A. Barhoum, T. A. Khattab, L. Gätjen and R. Wilken, *Cellulose*, 2019, **26**, 5437–5453.

36 D. M. Bishop, M. Randič and J. R. Morton, *J. Chem. Phys.*, 2004, **45**, 1880–1885.

37 R. G. Pearson, *Inorg. Chem.*, 1988, **27**, 734–740.